

Qualification of CuCr1Zr for the SLM Process

**E. Uhlmann¹, A. E. Tekkaya², V. Kashevko^{1*}, S. Gies²,
R. Reimann¹, P. John¹**

¹ Institute for Machine Tools and Factory Management IWF, Technische Universität Berlin, Germany

² Institute of Forming Technology and Lightweight Construction, TU Dortmund University, Germany

*Corresponding author. Email: kashevko@iwf.tu-berlin.de

Abstract

Working coils for electromagnetic forming processes need to comply with a wide list of requirements such as durability, efficiency and a tailored pressure distribution. Due to its unique combination of high strength and high electrical conductivity CuCr1Zr meets these requirements and is a common material for coil turns. In combination with conventional coil production processes like winding or waterjet cutting the use of this material is state of the art. A promising approach for coil production is the use of additive manufacturing (AM) processes. In comparison to conventional manufacturing processes, AM offers tremendous advantages such as feature-integration e.g. undercuts or lattice structures. However, this increased design freedom only leads to improved working coils if copper alloys with high strength and high electrical conductivity such as CuCr1Zr can be processed. Due to the high thermal conductivity and reflectivity the use of suchlike materials in additive manufacturing processes is challenging. Considering the effects of the required pre- and post-processing treatments for additive manufactured parts the need for research is further increased. The objective of this paper is to develop a method for the qualification of CuCr1Zr for the selective laser melting (SLM) process. This comprises the powder characterization, the process parameter identification and the microstructure investigation of the generated test geometries.

Keywords

Electromagnetic forming, Additive manufacturing, Selective laser melting

1 Introduction

Durability and efficiency are two basic requirements for working coils in electromagnetic forming operations (Belyy et al., 1977). Both aspects are mainly affected by the choice of the coil turn material. While a high yield strength is beneficial to withstand the mechanical loads a high electrical conductivity increases the process efficiency due to lower heating losses (Risch, 2008). A group of materials with a likewise high yield strength and electrical conductivity are low alloyed precipitation hardening copper alloys. With a yield strength in range of 300 to 400 MPa and an electrical conductivity of about 43 MS/m (74% IACS) (Deutsches Kupferinstitut, 2005) CuCr1Zr has a well-balanced property profile for working coils. In combination with conventional coil production processes like winding or waterjet cutting (Golovashchenko, 2006) the use of this material is state of the art.

Selective laser melting (SLM) is an additive manufacturing process and allows a layer by layer production of complex components directly out of metal powder based on CAD-Data. This technology offers tremendous advantages such as feature-integration e.g. undercuts, lattice structures for light weight construction as well as inner cooling channels. Today SLM is applied in the area of rapid prototyping, rapid tooling and rapid manufacturing. The most frequent manufactured products are tools and individual objects for the medical, automobile and aerospace industry (Gebhard, 2013). The relatively small range of suitable materials limits the broader application of the process. Already well known materials for SLM are stainless and tool steels, titanium-, aluminum- and nickel based alloys with powder grain sizes from 10 to 75 μm . To develop new applications for SLM, novel materials have to be qualified (Uhlmann and Urban, 2011). To qualify new materials for the SLM process different approaches were developed which are all based on a similar procedure. In the first stage maximization of the relative specimen density is the main objective. Afterwards, mechanical properties e.g. yield strength are analyzed and adjusted to reach values comparable to those of conventional wrought alloys. This could also include a heat treatment of the specimen. Finally, the process parameter set is optimized in terms of productivity (Uhlmann and Urban, 2012; Kempen et al., 2011; Sehart, 2010; Ahuja et al., 2014). In the field of SLM few research is focused on the processing of copper alloys. This can mainly be attributed to the difficulties that occur due to the high thermal conductivity and high reflectivity of copper. While the reflectivity of steel is in the range of $R_{\text{Fe}} \sim 0.64$, copper alloys reach values of up to $R_{\text{Cu}} \sim 0.99$ (Pogson et al., 2003). Zhang et al. (2014) reached a relative density of $\rho_{\text{rel}} = 94.6\%$ for specimen made of CuCr1Zr using a laser with a maximum power of 375 W. Becker et al. (2011) achieved densities of about $\rho_{\text{rel}} = 99\%$ with another copper alloy Hovadur[®] K220 (Schmelzmetall AG, 2006). However, they required significantly more laser power in the range of 1000 W. In summary, lack in the state of the art on the processing of CuCr1Zr with SLM was identified. The main issue is to achieve the relative density of $\rho_{\text{rel}} \geq 99\%$ for CuCr1Zr. The successful processing of CuCr1Zr allows production of working coils for electromagnetic forming and others applications.

2 Objectives

Main objective was to develop a knowledge base for processing CuCr1Zr using SLM. This includes the identification of process relevant parameters and copper-inherent characteristics regarding SLM e.g. heat dissipation through high thermal conductivity, oxidation, densification and porosity. Based on this investigation a set of parameters was derived to process CuCr1Zr with a relative part density close to $\rho_{rel} \geq 99\%$ (VDI 3405, 2014). This is the basic requirement for further investigations focusing on mechanical properties or the material performance in electromagnetic forming operations.

3 Approach

All specimen were produced on the SLM machine SLM 250^{HL}, MTT Technologies GmbH, Luebeck, Germany. An overview of the machine specifications is given in **Figure 1**.



Machine specifications:

Building space :	250 mm x 250 mm x 350 mm
Laser (cw):	400 W
Focal point diameter:	70 ... 300 μm
Layer thickness:	20 ... 100 μm
Particle size:	10 ... 65 μm
Building speed:	5 ... 20 cm^3/h
Tolerance:	± 50 μm (x, y, z)

Figure 1: Selective Laser Melting machine SLM 250HL

3.1 Powder Characterization

The inert gas atomized powder was classified into the grain size range of 20 to 63 μm and which was supplied by TLS Technik GmbH & Co. Spezialpulver KG, Bitterfeld, Germany. The powder properties were obtained from the suppliers' inspection certificate following European Standard DIN EN 10204, 2005 and validated by retesting upon receipt. The powder analysis was carried out according to VDI 3405-2, 2013 guidelines. Investigated powder requirements were grain size distribution DIN ISO 4497, 1991, grain morphology DIN EN ISO 3252, 2001 and bulk density DIN EN ISO 3923-1, 2010.

3.2 Parameter Identification

A three-stage qualification process was used to identify a suitable set of process parameters, **Figure 2**. Focusing on the most critical part quality indicators e.g. path width, wall thickness or relative density the process window was narrowed down further in each stage while the specimen geometry gets increasingly complex. For every stage a preheating temperature of $T_V = 200^\circ\text{C}$ was applied to reduce thermal stress and distortion.

The first stage covered a parameter field of 128 combinations for the production of single melt tracks of one layer thickness $\Delta z = 50 \mu\text{m}$ on a steel (H13, 1.2344) substrate plate. Varied parameters were the focal position x_F , which is linked to the beam diameter d_B , laser power P_L and scanning velocity v_s with 3 repetitions. Furthermore, a number of reference specimen were produced to assess and eliminate the effect of the specimen position in the test array. The melt tracks were analyzed via reflected-light microscopy. Path width, path uniformity, discolorations and balling were rated. Parameter combinations which yielded promising results were used for the further investigations. The adequate focal position $x_F = +1.0 \text{ mm}$ ($d_B = 80 \mu\text{m}$) was determined.




Stage 1	Geometry single scan paths on substrate 	Parameters beam diameter d_B laser power P_L scanning velocity v_s	No. of Test Specimens 561
	Evaluation optical inspection via light microscopy quality indicators: path width, path uniformity, discolorations, balling		
Stage 2	Geometry thin walls 	Parameters laser power P_L scanning velocity v_s	No. of Test Specimens 143
	Evaluation image processing of cross-sectional micrographs quality indicators: wall thickness, wall uniformity, adhesions		
Stage 3	Geometry cubes on supports 	Parameters laser power P_L hatch spacing Δy	No. of Test Specimens 15
	Evaluation digital processing of computer tomography data and inspection of micrographs quality indicators: relative density, microstructure		

Figure 2: Qualification process for CuCr1Zr

In the second stage were built thin walls with thickness of one melt path width, in the narrowed down parameter field from stage 1. The varied parameters were laser power P_L and scanning velocity v_s . The average wall thickness and its standard deviation as wells as number and size of adhesions were analyzed as quality indicators. The final parameter set for thin wall structures (support structures) was determined in this stage.

For the third stage cubes with a dimension $5 \times 5 \times 5 \text{ mm}$ were produced using a further narrowed down parameter field. The varied parameters were laser power P_L and scan spacing Δy . The specimen were evaluated by digital processing of computer tomography (CT) data. For investigations on this stage 15 combinations were chosen. The evaluation of the results yielded to a parameter combination for the production of dense volumes of CuCr1Zr.

3.3 Data Acquisition – Density

The numerical density data was extracted from cross-sectional images by digital image processing. The images were obtained by computer tomography (CT) with a ZEISS METROTOM 800, Carl Zeiss AG, Jena, Germany. The scanning parameters are shown in **Table 1**.

Parameter	Unit	Value	Parameter	Unit	Value
Prefilter copper	mm	0.25	No. of Projections	-	2100
Voltage	kV	130	Digital Gain	-	2.5
Current	μA	123	Binning	-	1 x 1
Exposure Time	ms	800			

Table 1: Computer tomography (CT) scanning parameters

The CT-data were obtained as a 3D density field with a spatial resolution of $7 \times 7 \times 7 \mu\text{m}^3/\text{voxel}$. This density field was sliced into a number of cross-sections which were sequentially evaluated. The optimal threshold to differentiate between material and voids was determined with the Otsu's method (Otsu, 1979). The quotient of pixels identified as material and the total pixel number yielded the relative density ρ_{rel} . The individual results were averaged over all sections in a measured volume of $3 \times 3 \times 3 \text{ mm}^3$ in the center of the cubes. The density determination method by CT was validated by evaluation of micrograph sections and Archimedes' Method.

3.4 Data Acquisition – Microstructure

Micrograph sections were produced by manual wet-sanding with grain sizes P50, P800, P1000, P1200 and P2400 on SiC-paper and polishing with diamond suspension with grain sizes $3 \mu\text{m}$, $1 \mu\text{m}$ and $0.25 \mu\text{m}$ and with a 10 % aqueous iron nitrate solution. Etching was carried out using a Klemm III etchant (100 ml distilled water, 11 ml saturated aqueous sodium sulfate solution, 40 g potassium metabisulfite) for 5 seconds. The produced micrograph sections were digitized using light microscope Olympus BX51, Olympus Corporation and scanning electron microscope ZEISS LEO 1455 VP, Carl Zeiss AG, Jena, Germany.

4 Results

4.1 Powder Properties

The optical inspection via SEM revealed uniformly spherical grain morphology with a low number of adhering satellite particles, **Figure 3a**. Very few particles exhibit an irregular shape or edges. The particle surface shows an even layer of oxidized material. The cross-sectional micrographs in **Figure 3b** display no inclusions of foreign materials or entrapments of gas (porosity). The microstructure is homogeneously and fine as shown in **Figure 3c**.

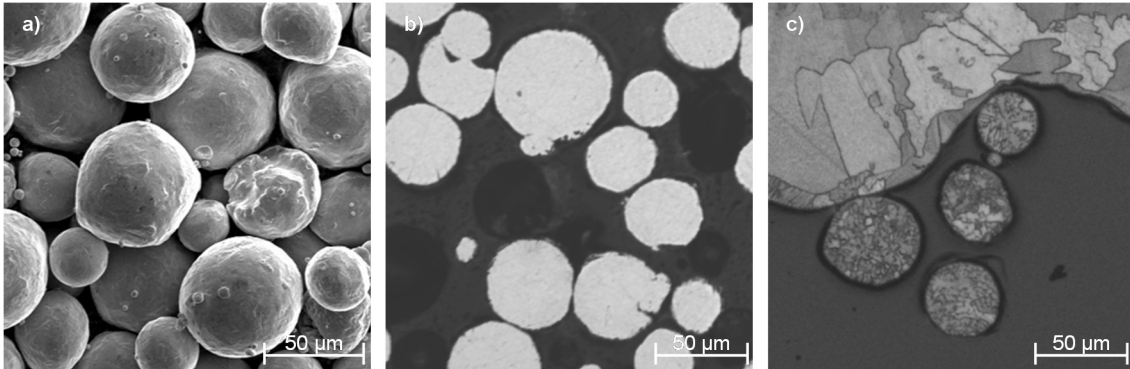


Figure 3: Optical powder inspection: a) particle morphology via SEM, b) porosity via microscopy and c) microstructure via microscopy of etched micrograph sections

4.2 Process Stability and Specimen Quality

Figure 4 shows SLM generated cubes with support structures on a steel substrate plate (H13, 1.2344). Optical inspection of the surfaces by eye reveals no differences in appearance. No discoloration due to overheating could be detected. The bonds of the support structures to the substrate and to the part are adequate which confirms the set of parameters chosen after stage 2. Therefore, the producibility of small-scale copper parts via SLM can be confirmed.

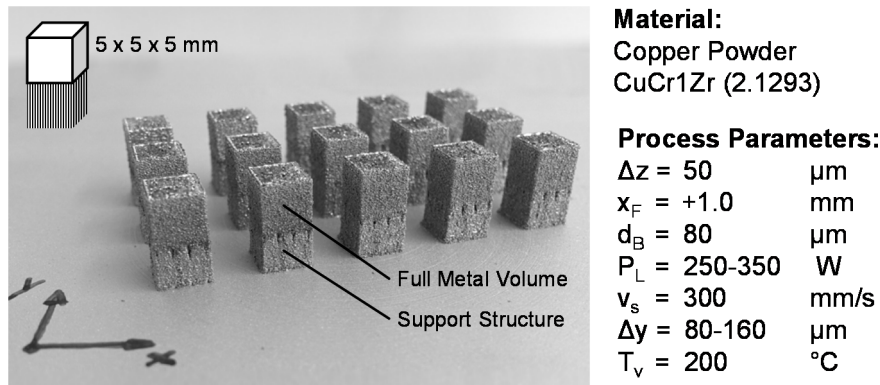


Figure 4: SLM generated cubes ($5 \times 5 \times 5 \text{ mm}^3$) on support structures

4.3 Densification and Porosity

The analysis of the cubes via CT yields to the data shown in **Figure 5**. Higher laser power P_L and reduced hatch spacing Δy result in increased densities. The highest achieved relative density was $\rho_{\text{rel}} = 99.5\%$. This confirms the expectation that the applied energy per volume E_V is the main influencing factor on the specimens' density. According to **Eq. 1** the energy per volume E_V is not only affected by laser power P_L and hatch spacing Δy but also by layer thickness Δz as well as scanning velocity v_s .

$$E_V = P_L / (v_s \cdot \Delta y \cdot \Delta z) \quad (1)$$

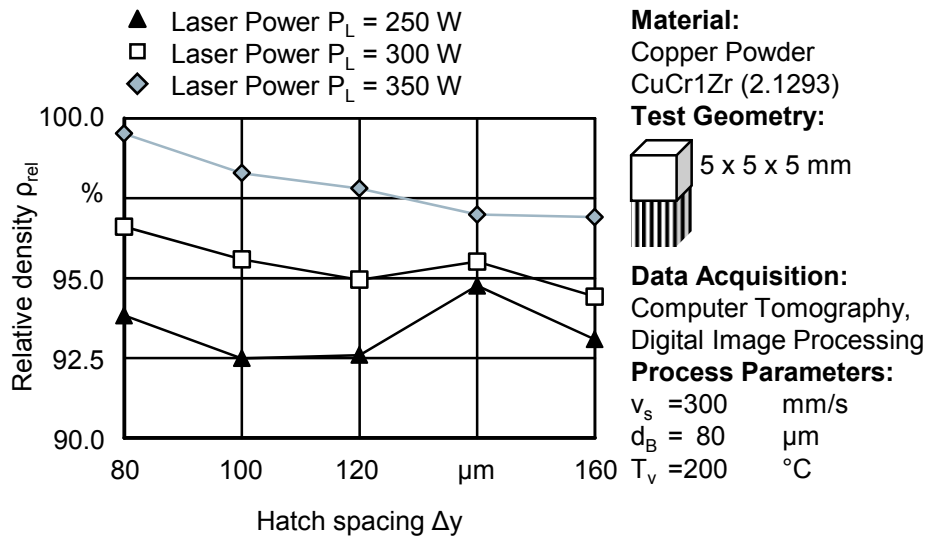


Figure 5: Achieved densities as a function of laser power P_L and hatch spacing Δy

The further results show an unusual variability at a hatch spacing of $\Delta y = 140 \mu\text{m}$. The phenomenon cannot be fully explained with the current amount of data but is not expected to have a huge impact on the identification of an optimal parameter set since the results indicate a maximum density ρ_{rel} at much lower hatch spacing.

4.4 Microstructure

The etched micrograph sections in **Figure 6** show randomized grain patterns with grains of distinctly different sizes ranging from $10 \mu\text{m}$ up to $200 \mu\text{m}$. The grains are elongated and show parallel patterns of multiple neighboring grains oriented in the same direction. They cross the boundaries of heat-affected zones of subsequent layers which can be seen as faint, half-circular lines (especially in the top right corner of **Figure 6c**). Some of the grains span multiple layers and seem to have alternating orientations about 45° to the build direction (z-axis). The grain pattern is disrupted by imperfections, such as porosity, and shows a refinement around the pore's edges. These pores span perpendicular to the build direction, which indicates suboptimal layer adhesion as the main reason for porosity. Furthermore, a number of smaller and rounder pores can be seen, which are expected to be caused by irregularities in the powder bed resulting in suboptimal densification and voids in the produced part.

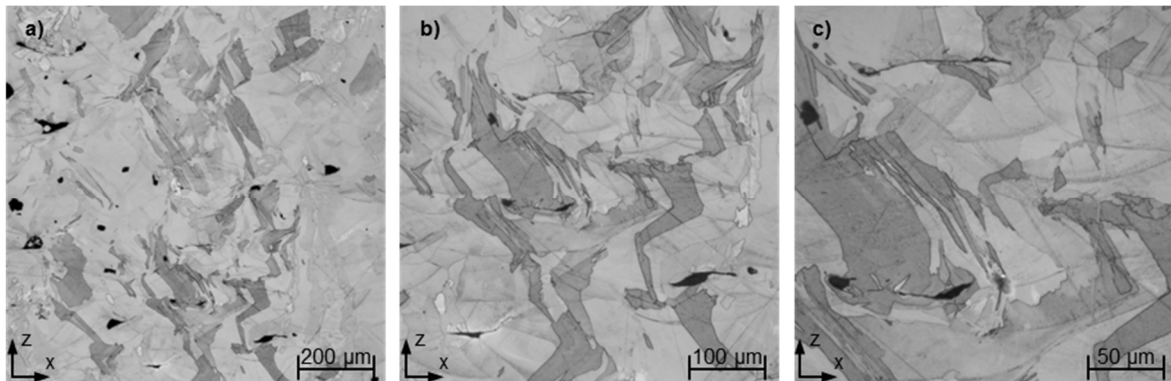


Figure 6: Light Microscopy of etched micrograph sections, process parameters: $P_L = 350\text{ W}$, $v_s = 300\text{ mm/s}$, $\Delta y = 80\text{ }\mu\text{m}$, magnifications: a) 50x, b) 100x, c) 200x

The SEM-scans in **Figure 7** confirm the assumptions above regarding the grain morphology and interaction with pores. The grains are distinctly elongated along the build direction (z-axis) and describe an alternating angle of $\pm 45^\circ$ to it. They stretch over the boundaries of heat-affected zones and are disrupted by pores. Especially **Figure 7a** proves that pores occur between layers. It seems as if the applied energy is insufficient so that the layer is not bonded to the previous layer in some areas. This is supported by the fact that **Figure 7a** shows powder particles that have not been molten inside the pores. Under maximum magnification of 10,000 times the precipitations in the copper alloy become visible. A punctual, homogenous distribution of extremely fine precipitations (diameter $D < 100\text{ nm}$) can be seen in the bulk of the material away from the heat-affected zone boundaries. In the vicinity of these boundaries the precipitations are bigger, more prevalent and form lattice structures. The precipitations are not uniformly distributed.

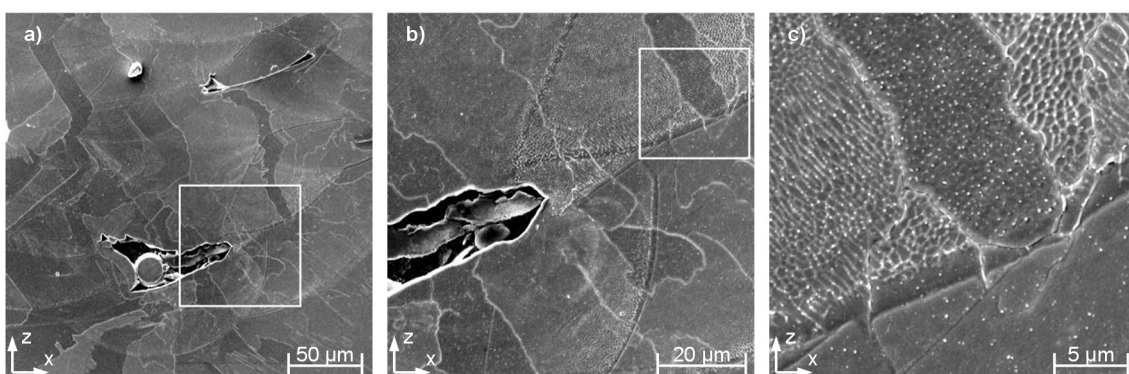


Figure 7: SEM of etched micrograph sections, process parameters: $P_L = 350\text{ W}$, $v_s = 300\text{ mm/s}$, $\Delta y = 80\text{ }\mu\text{m}$, magnifications: a) 1,000x, b) 3,000x, c) 10,000x

5 Conclusions

The identified process parameters facilitate the production of CuCr1Zr parts with a relative density of $\rho_{\text{rel}} > 99\%$ with a comparatively low maximum laser power of 350 W. This way the limitations of the material-machine-combination determined by Zhang et al. (2014) can be exceeded. Further research where required is needed to investigate the anomalies that occurred with a hatch spacing of $\Delta y = 140\ \mu\text{m}$.

The microstructure of CuCr1Zr shows pores that disrupt the homogenous grain patterns and a grain refinement around them. The grains are larger than usual with SLM due to the repeated application of high amounts of energy and the low-alloyed copper. The achieved microstructural state is not optimal for an artificial aging process because the precipitations are dispersed inhomogeneously and concentrated along the boundaries of heat-affected zones. Therefore, a solution annealing step is recommended before aging.

To complete the qualification process for CuCr1Zr analysis of the mechanical e.g. yield stress σ_y and physical properties e.g. electrical conductivity κ of the specimen are required. This also entails the analysis of the heat treatment procedure on these properties.

Acknowledgments

This paper is based on results acquired in the projects UH 100/174-1 and TE 508/51-1, which are kindly supported by the German Research Foundation (DFG).

References

- Ahuja, B., Karg, M., Nagulin, K. Y., Schmidt, M., 2014. Fabrication and Characterization of High Strength Al-Cu alloys Processed Using Laser Beam Melting in Metal Powder Bed. In: 8th International Conference on Laser Assisted Net Shape Engineering LANE 2014. Physics Procedia, S. 135 - 146.
- Becker, D., Meiners, W., Wissenbach, K., 2011. Generative Fertigung aus der Kupferlegierung Hovadur® K220 mittels Selective Laser Melting. Fraunhofer Institut für Lasertechnologie ILT, Aachen.
- Belyy, I.V., Fertik, S.M., Khimenko, L.T., 1977. Spravochnik Po Magnitno-impul' Snoy Obrabotke Metallov. Electromagnetic Metal Forming Handbook. English translation by Altynova, M. M.
- Deutsches Kupferinstitut, 2005: Material data specification CuCr1Zr. Online access: [https://www.kupferinstitut.de/fileadmin/user_upload/kupferinstitut.de/de/Document s/Shop/Verlag/Downloads/Werkstoffe/Datenblaetter/Niedriglegierte/CuCr1Zr.pdf](https://www.kupferinstitut.de/fileadmin/user_upload/kupferinstitut.de/de/Document%2FShop/Verlag/Downloads/Werkstoffe/Datenblaetter/Niedriglegierte/CuCr1Zr.pdf), last request: 22.12.2015.
- DIN EN 10204, 2005. Metallische Erzeugnisse - Arten von Prüfbescheinigungen. Berlin: Beuth.
- DIN EN ISO 3252, 2001. Pulvermetallurgie – Begriffe (ISO 3252:1999). Berlin: Beuth.

- DIN EN ISO 3923-1, 2010. Metallpulver- Ermittlung der Fülldichte – Teil 1: Trichterverfahren (ISO 3923-1:2008). Berlin: Beuth.
- DIN ISO 4497, 1991. Metallpulver; Bestimmung der Teilchengrößen durch Trockensiebung (ISO 4497:1983). Berlin: Beuth.
- Gebhardt, A., 2013. Generative Fertigungsverfahren. Additive Manufacturing und 3D Drucken für Prototyping - Tooling - Produktion. Unter Mitarbeit von J.-S. Hötter und M. Fateri. 4. Aufl. München: Hanser.
- Golovashchenko, S., 2006. Electromagnetic Forming and Joining for Automotive Applications. In: Proceedings of the 2nd International Conference on High Speed Forming, Dortmund, pp. 201-206.
- Kempen, K., Thijs, L., Yasa, E., Badrossamay, M., Verheecke, W., Kruth, J.-P., 2011. Process Optimization and Microstructural Analysis for Selective Laser Melting of AlSi10Mg. In: Solid Freeform Fabrication Symposium Proceedings. Solid Freeform Fabrication Symposium, Austin, USA, 08.08. - 10.08.2011.
- Otsu, N., 1979. A Threshold Selection Method from Gray-Level Histograms. In: IEEE Transactions on Systems, Man and Cybernetics, vol. 9, no. 1, pp. 62-66, Jan. 1979.
- Pogson, S.R., Fox, P., Sutcliffe, C.J., O'Neill, W., 2003. The production of copper parts using DMLR. Rapid Prototyping Journal. Vol.9:334-43.
- Risch, D., Nebel, J., Psyk, V., Vogli, E., Tillmann, W., Tekkaya, A. E., 2008. Hybrid Material Design for Coils used in Electromagnetic Forming Processes. In: Proceedings of the 7th International Conference “THE” Coatings in Manufacturing Engineering, pp. 269 – 278.
- Schmelzmetall AG. Material data specification HOVADUR® K 220. Issue Nr. 02DE, from 01.04.2006. Online access: http://www.schmelzmetall.com/wp-content/uploads/2015/06/hovadur_k220_vers02_de.pdf, last request: 22.12.2015.
- Sehrt, J., 2010. Anforderungen an die Qualifizierung neuer Werkstoffe für das Strahlschmelzen. In: Seminarbericht (2010) 97: Rapid Manufacturing, Universität Duisburg-Essen, Duisburg, Essen.
- Uhlmann, E., Urban, K., 2012. Approach for the Qualification of Novel Materials for Selective Laser Melting for the Example of Nickel-based Superalloy Diamalloy 4004NS. Direct Digital Manufacturing Conference 2012, Berlin, 14. - 15.03.2012.
- Uhlmann, E., Urban, K., 2011. Markt- und Trendstudie Laserstrahlschmelzen in der generativen Fertigung 2010. Schriftenreihe: Märkte kennen – Trends nutzen, Fraunhofer IPK, pp. 22.
- VDI 3405, 2014. Additive manufacturing processes, rapid manufacturing – Basics, definitions, processes. Berlin: Beuth.
- VDI 3405-2, 2013. Additive manufacturing processes, rapid manufacturing – Beam melting of metallic parts. Qualification quality assurance and post processing. Berlin: Beuth.
- Zhang, D. Q., Liu, Z. H., Chua, C. K., 2014. Challenges Involved in Selective Laser Melting of C18400 Copper Alloy. In: Fraunhofer Direct Digital Manufacturing Conference proceedings.